Should virus capsids assemble perfectly? Theory and observation of defects

Justin Spiriti[a], **James F. Conway**[b,1], **and Daniel M. Zuckerman**[a,1]

[a]Department of Biomedical Engineering, Oregon Health and Science University, Portland, OR 97239, United States; [b]Department of Structural Biology, University of Pittsburgh, Pittsburgh, PA 15260, United States

This manuscript was compiled on October 15, 2019

Although published structural models of viral capsids generally exhibit a high degree of regularity or symmetry, structural defects might be expected for several reasons: the finite-temperature, fluctuating environment in which capsids assemble, the maturation process many capsids undergo, and the requirement of some capsids for disassembly prior to genome delivery. Different lines of evidence also suggest the presence of defects: the observation of defective structures in computer simulations, and the presence of imperfect and off-pathway capsids in single-particle cryoEM studies. To begin quantifying the conditions under which defects might be expected, we extend prior work by developing a simple equilibrium theory for capsids based on a lattice model allowing for both ideal and defective sites. Both analytical and numerical calculations with the model show there is a fairly sharp threshold value for the difference in effective pair-binding affinities between ideally oriented and mixed ideal/defective pairs: below this capsid-specific threshold, there is an appreciable population of defective capsids. Even when defective sites are not allowed, there is generally some population of vacancies. Our theoretical analysis is bolstered by quantitation of single particles in cryoEM micrographs suggesting that $\gtrsim$15% of particles may be defective. Beyond furthering our understanding of structural heterogeneity in virus capsids, the findings suggest a non-traditional strategy for assembly inhibition by enhancing 'off-lattice' interactions among capsid proteins via adaptor molecules.

hepatitis B virus | capsid assembly | lattice model | cryoEM | structural defects

Capsid assembly is a critical step in the life cycle of all viruses(1, 2). During each infection cycle, capsids must assemble for each new viral replicate before it leaves the cell, and often must go through maturation steps that involve significant changes in conformation as well. One consequence of the dynamic and intrinsically stochastic nature of viral capsid assembly is that it does not always proceed to a precise end point and that occasionally defective capsids form. For example, there are three forms of the herpesvirus capsid that have been isolated in the nucleus, two of which do not proceed to form fully infectious virions.(3, 4) The human hepatitis B virus capsid can assemble in vivo into two structures with different numbers of quasi-equivalent subunits.(5) The symmetry may be either $T = 3$ (with 90 subunits per capsid) or $T = 4$ (with 120 subunits per capsid) depending on the conformational behavior of seven amino acid residues on the C-terminal region of the HBcAg capsid subunit.(6–8) The nature of the structures that form may also depend strongly on the ambient conditions. For example, the cowpea chlorotic mosaic virus (CCMV) can form a variety of structures, including multiwalled shells, tubes, and "rosettes", depending on the pH and ionic strength.(9)

The limitations of conventional structural biology tech-

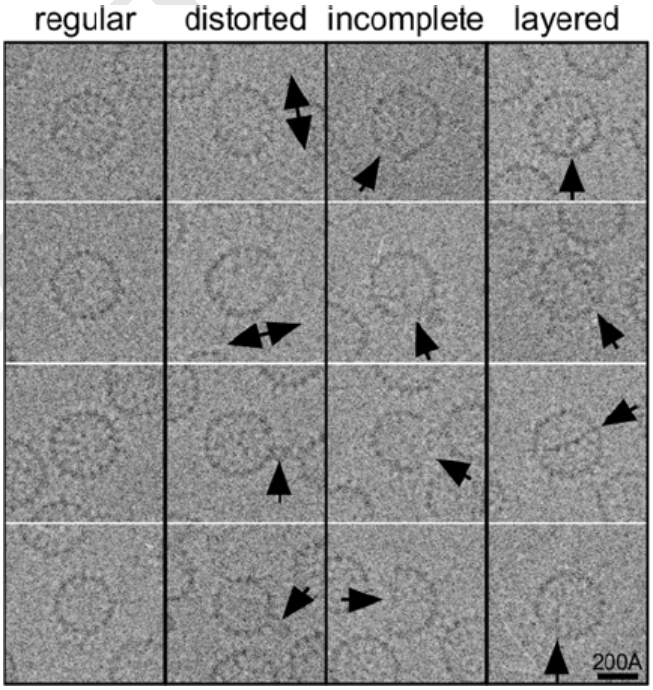

Fig. 1. Heterogeneity in raw cryoEM data. Selected cryoEM images of hepatitis B capsid particles. Arrows indicate structural variation.

DRAFT

niques make it very difficult to verify the formation of defective capsid structures directly. While structures of individual viral capsid subunits can be obtained by X-ray crystallography, most structures of complete capsids are obtained using cryoelectron microscopy (cryo-EM).(10, 11) Cryo-EM images often include capsids that are distorted or incomplete, or which have additional layers of subunits (fig. 1).(12) However, the signal-to-noise ratio of individual cryo-EM images is low, so obtaining atomistic structures requires collecting, filtering, re-orienting and averaging many such images.(13–16) This in turn requires discarding images of capsids that appear to be defective, and exploiting symmetry in the averaging process, which artificially imposes a corresponding symmetry on the resulting structure. Since defective capsids are not uniform, this method cannot be applied to calculate high resolution structures of defective capsids. Similarly, X-ray crystallography exploits the perfect repetition of the crystal lattice thus excluding observation of irregular or infrequent capsids resulting from defects in assembly.

In the work presented here, we choose to work with the hepatitis B virus (HBV) capsid as a demonstration system, because cryo-EM images of this capsid available to us show a variety of defects. Some of the defects represented include distorted, non-spherical capsids; incomplete capsids with gaps in their surface; and layered capsids with subunits forming additional surfaces inside an otherwise fully-formed capsid. Several instances of these defects are shown in figure 1. Importantly, HBV capsids assemble spontaneously from a solution of their subunit proteins, without genetic material, and have been the subject of extensive study (12, 17–19).

Computer simulations can enable detailed examinations of the mechanism of virus capsid assembly and the types of structures that can form.(20–24) Several simulations produced unusual, malformed structures, such as oblate capsids lacking icosahedral symmetry or aggregates composed of several partially formed capsids joined together in an irregular fashion.(25–29) A recent study of the assembly of the $T = 4$ form of the hepatitis B virus capsid using a semi-atomistic model yielded trajectories with persistent defects, despite the lowest energy conformation corresponding to a defect-free fully symmetric structure.(30)

Defective capsid formation can also be studied from a more theoretical perspective, focusing on thermodynamics and kinetics (1, 2, 31–34). A still-influential early model of equilibrium assembly for icosahedral capsids used 12 pentagonal subunits that unite to form a dodecahedron following a single, minimum-energy pathway for assembly.(31) This 12-pentamer model indicated that, for a range of plausible concentrations of free subunits, the population of intermediates was very low compared to that of either free subunits or complete capsids — i.e., two-state behavior: fully formed or monomeric. However, capsid subunits were considered rigid and able to exist in only two states: either fully attached to the capsid, or completely detached from it. Consequently, the only possible defects were vacancies. In addition, the assumption of a single minimum-energy pathway breaks down for large viruses because of the increased complexity of the structure and the larger number of sites where a subunit can be attached to a growing capsid. Some later theoretical work made highly similar assumptions to the 12-site model and reached similiar conclusions (33). Notably presaging some of the work reported here, a statistical mechanical lattice model has been developed for the assembly of the cowpea chlorotic mottle virus (CCMV) that could be used to study the thermodynamics of capsid assembly as a function of ionic strength and temperature.(35, 36)

Extensive experimental studies of the thermodynamics and kinetics of hepatitis B virus capsid assembly have been performed. (18, 31, 37) Significant concentrations of species with molecular masses intermediate between individual subunits and complete capsids were not reported, apparently confirming the two state picture of Ref. (31). However, the resolution of size exclusion chromatography and light scattering as mass-measurement techniques is insufficient to distinguish between complete, perfect capsids and those that have small defects or vacancies. That distinction is revisited here.

We take a statistical-mechanical approach to the problem of determining the equilibrium distribution of capsid states. Our model is similar to the lattice gas model for studying phase transitions in critical fluids,(38, 39) but defined on a contact graph that reflects the geometry of the HBV capsid. This model incorporates the possibility of capsid subunits being partially attached or being in a conformational state such that their interactions with a partially formed capsid are not as strong as the intersubunit interactions in a fully formed capsid. The model can be solved analytically under the approximation that defects in capsids are isolated, and can also be simulated numerically using the Metropolis Monte Carlo method.(40)

Using this model, we characterize the conditions under which capsid formation is thermodynamically stable, as a function of the chemical potential of free capsids and two interaction strength parameters representing the strength of interactions between fully attached subunits and between fully attached and partially attached subunits. We show that the proportion of defective capsids can be appreciable when the difference in these two interaction strengths is below a threshold. We further extend the analysis to other viruses by considering the relationship between this threshold, the number of subunits in a capsid, and the number of contacts each subunit

DRAFT

Significance Statement

Both computer simulations of icosahedral viral capsid assembly and cryoelectron (cryoEM) microscopy images of assembled capsids show that capsids sometimes assemble into defective structures of lesser symmetry. We found that about 15% of cryoEM images of single hepatitis B virus capsids show defective capsids. To begin to understand capsid defects on a quantitative basis, we developed a model with sites that can either be vacant, ideally occupied, or mis-occupied. Defects were generally found to occur, with a frequency dependent on the interaction strengths of ideally occupied sites and mis-occupied sites. Our results suggest that enhancing incorrect interactions between capsid proteins may be a way to diminish correct assembly.

J. F. C. and D. M. Z. designed research; J.S. contributed new reagents/analytic tools; J. S., J. F. C. and D. M. Z. performed research; J. S. and J. F. C. analyzed data; and J. S., J.F. C. and D. M. Z. wrote the paper.

The authors declare no conflict of interest.

[1]To whom correspondence should be addressed. E-mails: James.Conway@pitt.edu and zuckermd@ohsu.edu

makes. These results suggest that defective capsids can form in significant concentrations under a range of conditions.

1. Results

We first present analysis of cryoEM image data. Random sampling of single-particle images enables estimation of fractions of different types of defects and provides strong motivation for the theoretical analysis.

To probe the model, we present results from both Monte Carlo simulations and our analytical approximation, noting that the latter readily extends to arbitrary spherical capsids. We study the average and distribution of the sizes of partially formed capsids and the fraction of perfect capsids as a function of the three parameters of our model: μ, the chemical potential of free dimers with which the capsid is in equilibrium; $\Delta G_{\mathrm{ideal}}$, the strength of the interaction between ideally occupied sites; and $\Delta G_{\mathrm{mixed}}$, the strength of the interaction between an ideally occupied and a mis-occupied site. We compare these results to those from our analytical approach, which relies on the assumption that defects are isolated and therefore is expected to work best when capsid formation is strongly favored and only occasional defects occur. We then extend the predictions of the analytical model to other spherical capsid viruses.

A. Defective capsids in cryo-EM images. We collected images from three cryo-EM micrographs of HBV capsids, and examined samples of images manually to determine whether they contained defects and what kinds of defects they were. We examined both the entire stack of images obtained by template-based autopicking, as well as a filtered subset obtained by 2D classification. Table 1 summarizes the results of this investigation. The samples of images themselves are shown in figures S1 and S2 and descriptions of which images exhibit what kinds of defects are shown in tables S1 and S2 in the Supporting Information. The template-based autopicker selected a large number of image centers that were located midway between several capsid particles, resulting in images that consisted of parts of multiple capsids. Almost all of these images were filtered out by the 2D classification.

About one-sixth of the images from the filtered stack have visible defects. A much larger proportion of the images in the original stack also show defects; some of these images could have been filtered out by the classification steps that were used to create the filtered stack. In any case, there is a high percentage of defects present – at least one in six particles is defective, and this is likely an underestimate because of the use of template-based autopicking of particles using perfect capsids as templates. We note that only 600 of 1618 total T=4 capsid particles were used in the original structure publication(12) due primarily to technological constraints, but likely resulting in a selection of the best one-third of the particle dataset and avoiding the defective capsids.

The cluster mean images obtained by automatic 2D classification of the filtered stack are shown in figure 2 and the distribution is shown in table 2. During the classification, some of the clusters became empty, so that RELION produced a total of 22 clusters at the end of the E-M iterations. Almost all the images (98.5%) were classified into a set of clusters representing "perfect" capsids (clusters 11, 16, 24, 26, 29, 30, 32, 41, and 46). RELION did identify a few clusters that appear to represent defective capsids. For example, cluster 47 appears to contain HBV capsids that are missing a dimer along the outer edge as seen in the micrograph, while cluster 42 appears to contain incomplete capsids that are missing multiple such dimers, similar to those shown in the "incomplete" column of figure 1. Clusters 35 and 45 appear to contain elongated capsids similar to those portrayed in the "distorted" column of figure 1. However, these clusters together account for only 1.5% of the filtered stack. It appears that many of the images that were manually classified as defective were placed by RELION in the "perfect" clusters, and were then averaged out by other images. Alternatively, the individual images are noisy, and some of the defects identified by manual inspection may in fact be a result of that noise. Still, despite these differences, it is clear that at least 1%, and possibly more, of the images from the filtered stack represent defective capsids, as determined by classification using RELION.

Table 1. Summary of number and type of defective capsids found in samples taken from the two classes of images identified from electron micrographs of the HBV capsid. Descriptions of individual images are shown in table S1 for the entire stack and table S2 for the filtered stack. The images themselves are shown in figure S1 for the entire stack and figure S2 for the filtered stack.

Stack	Entire	Filtered
Total number of images in stack	17790	4940
Sample size	100	100
Images containing parts of multiple capsids	64	0
Images not containing a visible capsid, or partially obscured	3	1
Images showing extra lines, additional dimers, or "buds"	0	8
Images with one missing dimer	8	7
Images with multiple missing dimers	2	0
Images with an elongated or non-circular capsid	2	0
Images with unusually small capsids	4	0
Images with small capsids that also have a missing dimer	5	0
Total fraction of defective capsids	17.0%	16.0%

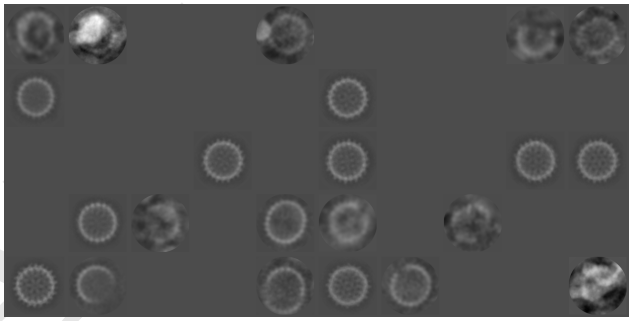

Fig. 2. Cluster means obtained from automatic 2D classification of the filtered stack.

B. Structural heterogeneity in the hepatitis B viral capsid model. Turning to the graphical model of Fig. 3, we first confirm that the average number of occupied sites depends on μ and $\Delta G_{\mathrm{ideal}}$ (for $\Delta\Delta G = 0$) as expected. Figure 4 indicates that capsid formation is more favorable for a higher μ (implying a higher concentration of free subunits in equilibrium with the capsids) and for higher $\Delta G_{\mathrm{ideal}}$ (stronger interactions between subunits). Plots with other values of $\Delta\Delta G$ (shown in figure S4 in the Supporting Information) were very similar to

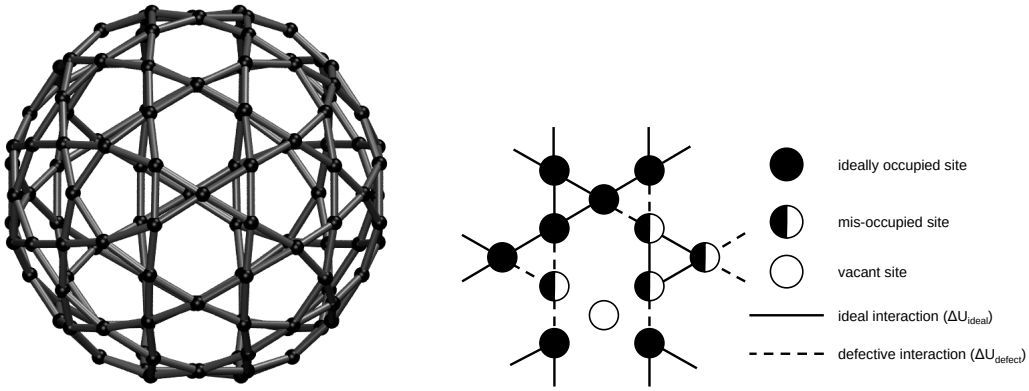

(a) **(b)**

Fig. 3. Lattice model for Hepatitis B virus capsid. (a) The perfect capsid, with all sites ideally occupied. (b) F showing ideally occupied sites (black circles), mis-occupied sites (black half-circles), and vacant sites (white circles). The interaction energy between ideally occupied sites or between mis-occupied sites is $\Delta G_{\rm ideal}$ (solid line), whereas the interaction energy between an ideally occupied and a mis-occupied site is $\Delta G_{\rm mixed}$ (dotted line).

Table 2. Distribution of images in clusters obtained from automatic 2D classification of the filtered stack. Clusters are numbered so that clusters 1-10 correspond to the first row of figure 2, 11-20 to the second row, and so on.

Cluster	Number of images
1	1
2	2
5	1
9	1
10	1
11	250
16	358
24	525
26	451
29	569
30	584
32	605
33	1
35	18
36	1
38	1
41	1041
42	34
45	7
46	481
47	7
50	1

that shown in figure 4, implying that the average number of occupied sites does not vary much with $\Delta\Delta G$.

The model makes valuable predictions regarding structural heterogeneity. Figure 5 shows the actual distribution of the number of occupied sites for selected points in the $(\mu, \Delta G_{\rm ideal})$ plane. Most importantly, there is always some population of imperfect capsids, and this becomes dominant in some regions of parameter space. It is clear that, while the average number of occupied sites depends only weakly on $\Delta\Delta G$, the actual distributon of capsid sizes can vary significantly. For the chosen sets of parameters, the distributions have two peaks, one corresponding to a nearly fully formed capsid, the other corresponding to an isolated subunit. The probability minimum between these peaks increases with $\Delta\Delta G$, which we ascribe to entropic effects. Adding a third state increases the number of possible configurations, and in particular for larger capsids, there are more ways to mix fully-occupied and mis-occupied states. Consequently, the entropy associated with the largest capsids is greater when there is a mis-occupied state whose energy is close to that of the fully occupied state, $\Delta G_{\rm mixed} \sim \Delta G_{\rm ideal}$; therefore larger capsids will be favored.

When do structurally *perfect* capsids predominate? We studied the proportion of perfect capsids, where all sites are ideally occupied, and compared results from the Monte Carlo simulations to the analytical results obtained using the isolated-defects approximation (eq. 9). Figure 6 shows this proportion as a function of μ, $\Delta G_{\rm ideal}$, and $\Delta G_{\rm mixed}$, with plots in the $(\Delta G_{\rm ideal}, \Delta G_{\rm mixed})$ plane. The proportion of perfect capsids depends predominantly on the difference $\Delta\Delta G = \Delta G_{\rm mixed} - \Delta G_{\rm ideal}$, and shows a critical threshold of $\Delta\Delta G \approx 2.5 k_B T$. Above this threshold, and for a sufficient interaction strength, structurally perfect capsids predominate, while below this threshold, the fraction of defective capsids can become significant. As $\Delta\Delta G$ approaches zero, the many imperfect but complete capsid configurations in which some sites are mis-occupied, but no sites are vacant, come to have

DRAFT

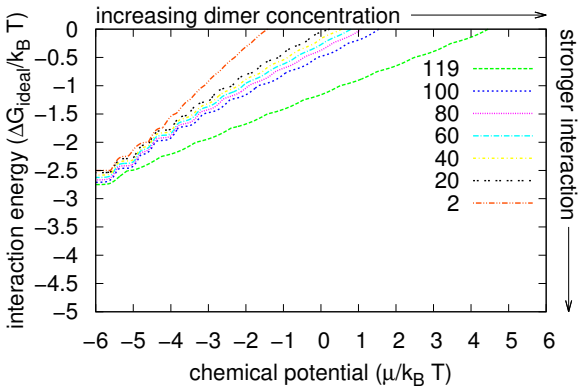

Fig. 4. Dependence of capsid formation on chemical potential μ and interaction strength ΔG_{ideal}. Contour plot of the average connected capsid size (including mis-occupied sites) in Monte Carlo simulations of our model on the HBV capsid contact graph in the $(\mu, \Delta G_{\text{ideal}})$ plane for $\Delta\Delta G = 0$. Plots for other values of $\Delta\Delta G$ are found in figure S4 of the Supporting Information. Note that for ideal solutions $\Delta\mu \sim -k_B T \ln[\text{dimer}]$. Higher concentrations and stronger interactions lead to more fully formed capsids.

the same energy. Consequently, the distribution of configurations is dominated by imperfect capsids for entropic reasons, and the probability of a perfect capsid is infinitesimally small for $\Delta\Delta G = 0$. The threshold of $2.5k_BT$ represents the point at which the lower energy of an ideally occupied site outweighs this entropic effect. The plots of results from the Monte Carlo simulations are nearly indistinguishable from the analytical results.

The value of ΔG_{defect} has little impact on the probability of perfect capsids, as demonstrated by plots of the perfect capsid probability for various values of ΔG_{defect} (figure S6). Note that because it is the interaction energy between adjacent mis-occupied sites, ΔG_{defect} cannot appear in an analytical approximation that assumes that all the defects are isolated. As shown in the SI, ΔG_{defect} does appear in second-order and higher terms in the virial expansion corresponding to defects in which two mis-occupied sites are adjacent to each other.

C. Model prediction for arbitrary spherical capsids. We extended our analysis to arbitrary spherical viral capsids using equation 9, a mathematical relationship between N and k, which are the geometric properties of a viral capsid, and the energy difference $\Delta\Delta G$ needed for the formation of defective capsids. Under the conditions favoring capsid formation, μ is large and positive and there are strong interactions between ideally occupied sites; consequently, the term $\exp[-(\mu - k\Delta G_{\text{ideal}})/k_BT]$ is relatively small. If we drop this term and invert the remaining equation in terms of $\Delta\Delta G$ we obtain an expression for the threshold value of $\Delta\Delta G$ below which the fraction of defective capsids p_{perf} exceeds a specified threshold:

$$\Delta\Delta G/k_BT = -\frac{1}{k}\log\left(p_{\text{perf}}^{-1/N} - 1\right) \qquad [1]$$

Figure 7 shows plots of this expression in the (N, k) plane for $p_{\text{perf}} = 0.99$ and 0.95, along with values of N and k for several viruses. The formation of defective capsids is easiest (the threshold value of $\Delta\Delta G$ needed for the formation of defective capsids is least) for viruses with a large number of subunit in which each subunit has few neighbors. It is hardest to form defects in viruses with few subunits in which each subunit has many neighbors.

2. Discussion

A. Comparison with prior work. We are unaware of any previous quantitative analysis of the defective particles present in cryoEM micrographs, which are usually rejected for being quite variable in structure and presumed to be physiologically off-pathway. Nonetheless, they may constitute a sizable proportion of the sample under study reflecting the innate assembly fidelity of the complex as well as aspects of sample preparation, and may offer insights into assembly that could be exploited for anti-viral or other therapeutic purposes. Such heterogeneity in cryoEM structures is now taken to be a fundamental part of structural biology(41–44) and we hope that our findings will motivate similar analyses of other systems and other datasets.

Our theoretical model, while still greatly simplified, advances prior theoretical work in several ways. Generally speaking, our model incorporates more realistic and combinatoric possibilities than the seminal early model of Zlotnick (31) and follow-up work (33). We also find two-state behavior – mostly assembled and mostly disassembled – but the greater granularity of our model clearly shows that what appeared to be a uniform assembled state in the prior work consists of an *ensemble* of nearly fully assembled configurations in large parts of parameter space. That is, defects are common, both as vacancies and/or mis-assembled sites.

A model somewhat similar to ours has been used to study the assembly of CCMV.(35, 36) This model incorporates a grand-canonical term and a hydrophobic interaction term with the same forms as the two terms in equation 10. However, explicit electrostatic interactions, as well as the use of only vacant and ideally occupied sites (no mis-occupied sites), distinguish the CCMV model from ours. Despite these differences, the authors find distributions of capsid sizes that are two-peaked with the higher peak not being at full assembly, similar to those shown in figure 5 for our model.

In experimental studies of HBV capsid assembly, only two populations were observed using size-exclusion chromatography, but significant caveats apply. Species' molecular weights were measured using light scattering and corresponded to complete capsids and free dimers.(18) This is broadly consistent with our Monte Carlo simulations, which in most cases produce capsid size distributions peaked around either 1 dimer or 120 dimers, corresponding to a free dimer or a complete capsid respectively. In a few cases we observe a distribution containing peaks corresponding to both sizes. The observation of only two peaks would seem to rule out significant concentrations of defective or partially assembled capsids. However, the experimental data is not sufficient to support this conclusion, because size-exclusion chromatography relies on hydrodynamic volume, not molecular weight, to resolve macromolecules,(45) and capsids with localized defects (such as missing dimers) would be expected to have a hydrodynamic volume very close to those of perfect capsids. Furthermore, interpretation of light scattering is based on the assumption that the particles detected are spherical with a refractive index that differs slightly from that of the surrounding medium.(46) Conse-

DRAFT

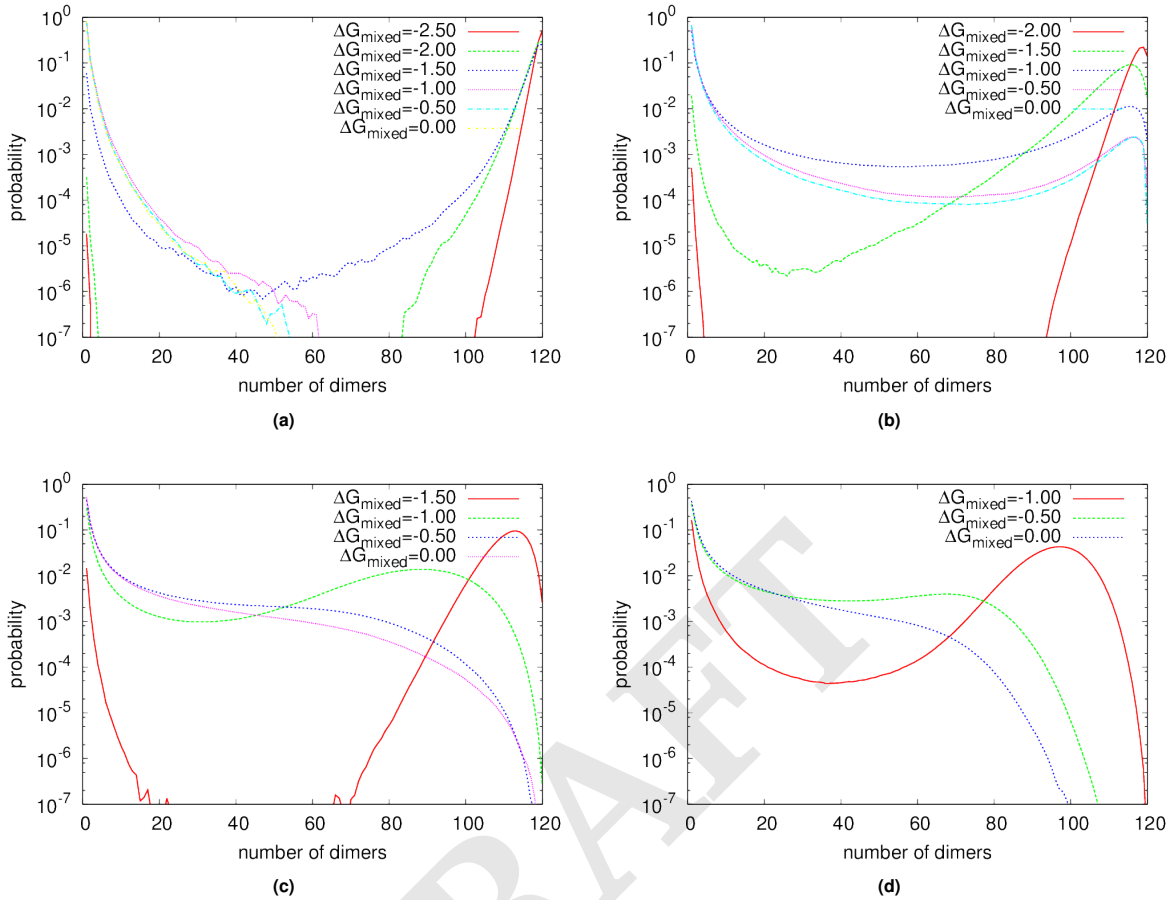

Fig. 5. Effect of defective sites on the distribution of partial capsid sizes. Distribution of the connected capsid size as a function of $\Delta G_{\mathrm{mixed}}$ for selected points in the $(\mu, \Delta G_{\mathrm{ideal}})$ plane. Points were chosen where the distribution of capsid sizes showed two peaks corresponding to nearly-complete capsids and isolated dimers. (a) $(\mu, \Delta G_{\mathrm{ideal}}) = (-5.0, -2.5)$; (b) $(\mu, \Delta G_{\mathrm{ideal}}) = (-4.0, -2.0)$; (c) $(\mu, \Delta G_{\mathrm{ideal}}) = (-3.0, -1.5)$; (d) $(\mu, \Delta G_{\mathrm{ideal}}) = (-2.0, -1.0)$. Once $\Delta\Delta G \gtrsim 1 k_B T$, there is an appreciable population of partially formed capsids and even a depletion of full capsids for weaker interaction strengths.

DRAFT

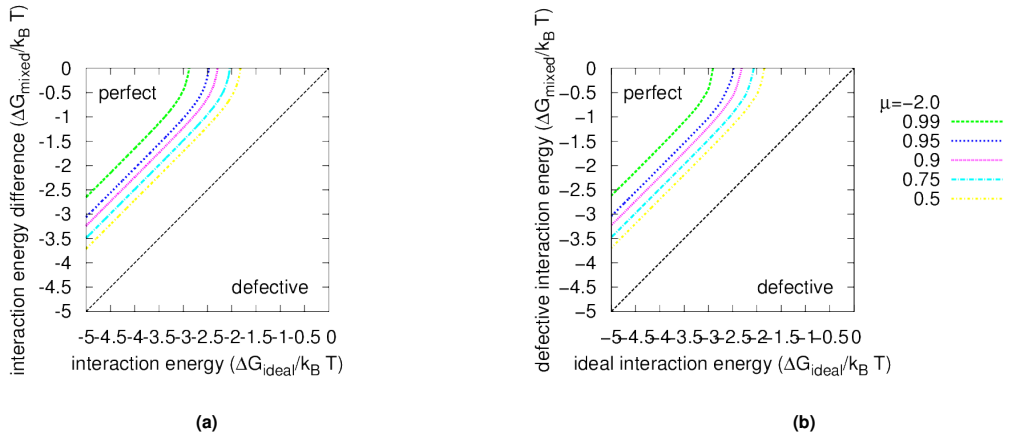

Fig. 6. When are perfect capsids expected? (a) Contour plots of the fraction of perfect capsids p_{perf} as determined from equation 9 and (b) p_{perf}, as determined from MC simulations, both in the $(\Delta G_{\mathrm{ideal}}, \Delta G_{\mathrm{mixed}})$ plane (chemical potential and ideal interaction energy) for $\mu = -2.0 k_B T$.

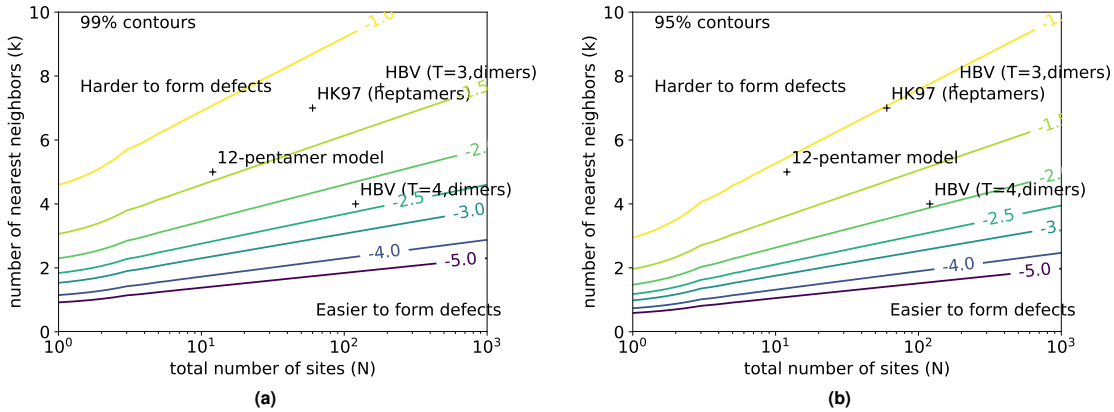

Fig. 7. Summary plot for arbitrary spherical viruses. Dependence of the threshold value of $\Delta\Delta G$ needed to ensure a high proportion of capsid formation on the total number of subunits in the capsid N and the number of nearest neighbors k, based on equation 1. (a) 99% capsid formation; (b) 95% capsid formation. Values of N and k for selected viruses are plotted as well. "12-pentamer model" refers to reference (31).

quently, the observed population corresponding to complete capsids may also include defective capsids that are nearly complete – i.e., species which may be of great biological importance.

A.1. An alternative inhibitor-design strategy. Our model has implications for the design of inhibitors of virus capsid assembly, which have received significant interest as a novel class of therapeutics for HIV(47–49) as well as for HBV.(50–52) The model suggests that it is possible to design two distinct types of inhibitors: ones that block or destabilize ideal interactions between capsid subunits, and ones that stabilize non-ideal interactions. In the case of HIV, both of these kinds of inhibitors have been developed (47–49). Coarse-grained simulations of the HIV-1 capsid protein suggest that the capsid assembly inhibitor PF74, a tripeptide mimic,(53) works by stabilizing trimers of dimers, which then interact with partially assembled capsids in such a way as to encourage them to form incorrect assemblies.(49) For HBV, the focus has been on developing modulators of capsid assembly that may either accelerate or inhibit functional capsid assembly, depending on circumstances. For example, the inhibitor BAY-41-4109 exhibits different behaviors depending on the stoichiometric ratio relative to the capsid dimers. At a low ratio it accelerates capsid growth, whereas at a higher ratio it causes capsids to misassemble into "voids" or polymers.(54). There is a binding site on the capsid for assembly modulators that can either trigger assembly or disassembly, depending on how the modulator is bound and what conformation it adopts.(55) Knowledge of the principles behind assembly should be useful for guiding the design of inhibitors that block or hijack the capsid assembly process.

B. Model limitations and avenues for future development. One limitation of the statistical-mechanical model described here is that it considers the formation of only one capsid at a time from a gas of free subunits. The possible defects are limited to vacant sites or sites with partially attached subunits. In other simulations, using structurally more realistic models, more complex structures were formed. For example, the Brooks group obtained a variety of irregular capsids, including twisted, tubular, prolate and conical capsids, as well as partially formed capsids with missing subunits and open misaggregates consisting of two partial capsids joined together.(26, 27) It is not obvious how to extend a model of the type presented here to accommodate irregular capsids or misaggregates. Nevertheless, the value of a tractable model is significant, as shown by our results.

The parameter ΔG_{ideal}, the interaction free energy, must include all environmental factors, including temperature and ionic strength. The experimental values for the interaction strength among HBV capsid subunits range from approximately -3.2 to -4.4 kcal/mol,(18) which correspond to values of ΔG_{ideal} from approximately -5 to -7 k_BT, on the upper end of the values considered here. The lower values are more consistent with physiological conditions; the strength of the intersubunit interaction increases with increasing temperature and ionic strength because of the primarily hydrophobic nature of the forces that hold the capsid together. Experimental studies comparing woodchuck and human HBV also demonstrate that the two capsid proteins, despite having approximately 65% sequence identity and forming very similar assembled capsid structures, have very different thermodynamics of assembly, with that of woodchuck HBV having a stronger entropic contribution to assembly.(19) In previous simulations, stronger interactions are usually used in order to speed up capsid formation. In the simulations performed by Hagan and Chandler, a "hysteresis" effect was observed(28) in which it was necessary to use a somewhat smaller interaction strength (about $12k_BT$) to cause fully assembled capsids to disassemble, compared to the interaction strength needed to assemble capsids from free subunits (about $16k_BT$). In our own simulations,(30) the energy of an intersubunit interaction is about 8 kcal/mol per intersubunit interaction, or about $13.3k_BT$ where $T = 300$ K is the simulation temperature.

3. Conclusions

To investigate systematically the potential for defect formation in virus capsids, we developed a statistical mechanical model that incorporates more realistic capsid geometry than prior work, as well as taking into account the possibility of

DRAFT

weaker intersubunit interactions due to partial attachment of subunits. The model is motivated by the substantial fraction of defective particles (∼1 in 6) occurring in a re-analyzed set of micrographs.

Both analytical approximations and Monte Carlo simulations of the model reveal that significant proportions of defective capsids can form when the difference in strengths between ideal and defective subunits is below a threshold that depends only on geometric properties of the capsid. This implies that capsid assembly can be inhibited equally well by blocking ideal interactions or by stabilizing non-ideal ones. While significant work remains to be done in extending the model to allow a greater variety of defects, and in clarifying the physical meaning of the parameters, these results demonstrate that the concentration of defective capsids can be more significant under certain conditions than previously appreciated.

4. Materials and Methods

A. Analysis of defective images in cryo-EM micrographs of HBV capsids. Three historical micrographs of the HBV capsid assembled from expressed HBcAg truncated at residue 147(6, 12) were analyzed to identify and classify images of defective capsids. Briefly, samples were rapidly vitrified on copper grids with lacey carbon film, transferred on a Gatan 626 cryoholder (Gatan, Pleasanton, CA) into a Phillips CM200 cryo-electron microscope (FEI/ThermoFisher, Portland, OR) operating at 120 kV, and imaged by low-dose techniques at 38,000x on film. The data were digitized on a SCAI flatbed scanner (Z/I Imaging, Huntsville, AL) to yield a pixel size at the sample of 1.84 Ångstroms. Scans of the three micrographs (which included one used in ref. (12)) were then trimmed and processed using ImageMagick (https://imagemagick.org) to remove the edges and to eliminate the data window imprinted on the micrograph, in order to reduce spurious regions of high contrast that would otherwise interfere with subsequent particle picking and extraction. The modified micrograph scans were then converted to MRC format using `em2em` (Image Science Software GmbH, Berlin, Germany) for further processing.

Images of capsids were then picked and extracted from the micrographs using RELION.(14, 56, 57) An initial set of 89 particles was manually picked and extracted from the micrographs, and subjected to 2D classification into 5 classes; one of the class means was then used as a template for template-based autopicking. A threshold value of -0.6 was used to maximize the number of particles selected while excluding unwanted debris as much as possible. This resulted in a first stack of 17790 particle images, which was subjected to 2D classification into 10 classes to remove partial capsids and other debris. Two of the classes were selected to provide a final filtered stack of 4940 images. A random sample of 100 images was then drawn (without replacement) from this stack and examined manually in order to identify any visible defects. Statistics on the types of defects visible in the sample of images were then collected. The filtered stack was also subjected to 2D classification with 50 initial clusters and 50 iterations of the expectation-maximization (E-M) algorithm used by RELION.

B. Model for capsid formation. We construct a statistical-mechanical model for capsid assembly and examine its equilibrium behavior, which depends only on the energy function via its parameters. Given a constant chemical potential for free subunits, we can determine the distribution of sizes of partially formed capsids. We emphasize that we are not estimating the free-energetic parameters of the model, but rather exploring the consequences of a physically plausible range of parameter choices.

Physically, each discrete state of our model represents a *set* of continuum configurations in the underlying configuration space. Therefore, all state energies are intrinsically *free* energies that account for both energetic and entropic characteristics of the underlying configurational sub-ensembles (58).

We employ a simple lattice-like graphical model with N sites (fig. 3), in which each site i can be in one of three states: unoccupied, "ideally" occupied (i.e. in the orientation suitable for the symmetric capsid), or mis-occupied (i.e. occupied but mis-oriented compared to the symmetric configuration). A contact graph $\mathcal{G}$ (fig. 3) shows which sites interact with each other. Thus the free energy of a capsid configuration $\mathbf{x}$ is given by

$$G(\mathbf{x}) = \sum_{\text{edges } ij \in \mathcal{G}} \Delta G_{\text{int}}(x_i, x_j) \qquad [2]$$

where $\Delta G_{\text{int}}(x_i, x_j)$ is an interaction free energy that depends on the occupation states x_i and x_j of the two sites i and j as given below.

The interaction energy ΔG_{int} can take on one of three possible values: ΔG_{ideal}, for interactions between ideally occupied sites, ΔG_{mixed} for interactions between a ideally occupied site and a mis-occupied site, or ΔG_{defect} for interactions between mis-occupied sites. In general, we expect that interactions between ideally occupied and mis-occupied sites will be weaker than those between ideally occupied sites. We defined the difference $\Delta\Delta G = \Delta G_{\text{mixed}} - \Delta G_{\text{ideal}}$ to be the difference between the two interaction energies and is always assumed positive – i.e., mixed interactions are weaker than ideal. We also assumed that the interaction between two adjacent mis-occupied sites (ΔG_{defect}) would be slightly weaker than that between ideally occupied sites (ΔG_{ideal}), so that $\Delta G_{\text{defect}} = \Delta G_{\text{ideal}} + 1.0 k_B T$. This difference was chosen based on the premise that the interactions between mis-occupied sites would be weaker than those between ideally occupied sites. Note that all of these interaction energies account for average effects of configurational fluctuations and hence represent effective free energies.

The probability of any given configuration $\mathbf{x}$ can be calculated based on its free energy. In order to probe the distribution of the number of occupied sites both in terms of energetic parameters and concentration effects, we work in the grand canonical ensemble, in which the chemical potential of capsid subunits μ is fixed and the number of assembled subunits self-adjusts accordingly. This corresponds to considering any partially-formed capsid as being in equilibrium with an ideal solution of free subunits. The probability of a given configuration $\mathbf{x}$ is given by

$$p(\mathbf{x}) \propto \exp[-\beta G(\mathbf{x})] \exp[-\beta \mu N(\mathbf{x})] = \exp\{-\beta[G(\mathbf{x}) - \mu N(\mathbf{x})]\} \qquad [3]$$

where $N(\mathbf{x})$ is the number of occupied sites for configuration $\mathbf{x}$. The total probability of having M subunits in the capsid is obtained by summing over all configurations having M

DRAFT

$$\Xi = e^{-G_{\rm perf}/k_BT} \sum_{N_v,N_m=0}^{N} \frac{N!}{N_v!N_m!(N-N_v-N_m)!} \exp\left[-\left(N_v\,\Delta G_{\rm vac} - N_m\,\Delta G_{\rm mis}\right)/\,k_BT\right] \quad [7]$$

$$p_{\rm perf} = \frac{e^{-G_{\rm perf}/k_BT}}{\Xi} = \left(\frac{1}{1+\exp[-(\mu-k\Delta G_{\rm ideal})/k_BT]+\exp[-k\Delta\Delta G/k_BT]}\right)^N, \quad [9]$$

occupied sites:

$$p(N) = \frac{\sum_{\mathbf{x}\ \text{s.t.}\ N(\mathbf{x})=M} \exp\{-\beta[G(\mathbf{x})-\mu N(\mathbf{x})]\}}{\sum_{\mathbf{x}} \exp\{-\beta[G(\mathbf{x})-\mu N(\mathbf{x})]\}} \quad [4]$$

The chemical potential μ is usually approximated by an ideal relation to concentration:

$$\mu = k_BT \ln \frac{[\text{subunit}]}{[\text{subunit}]_{\rm ref}} \quad [5]$$

though the true dependence is generally more complicated (59). The functional form of μ does not affect the results presented below.

C. Approximate analytical approach based on assuming isolated defects. It is possible to obtain an analytical expression for the partition function of this model if we make the approximation that all defects (either empty sites or mis-occupied sites) are isolated from each other. This is a good approximation if there are few defects, which is the regime of primary interest in which capsids are generally stable.

The free energy changes for each type of defect, a vacancy or mis-occupied site, can easily be obtained for a model with N sites, each of which has k nearest neighbors. Starting from a perfect capsid of free energy $G_{\rm perf} = -N\mu + (Nk/2)\Delta G_{\rm ideal}$, changing one site to empty removes the interactions along k edges, and the free energy change is $\Delta G_{\rm vac} = \mu - k\Delta G_{\rm ideal}$ If instead we change one site to a mis-occupied site, the free energy difference is $\Delta G_{\rm mis} = k\Delta G_{\rm ideal} - k\Delta G_{\rm mixed} = -k\Delta\Delta G$

The partition function can now be obtained from straightforward combinatorics. The number of configurations with N_v vacant sites and N_m mis-occupied sites is $\frac{N!}{N_v!N_m!(N-N_v-N_m)!}$. When all defects are assumed to be isolated (not neighboring another defect), the free energy difference from the perfect capsid is simply additive,

$$N_v\Delta G_{\rm vac} + N_m\Delta G_{\rm mis}\ . \quad [6]$$

The grand canonical partition function is then given by which is a trinomial form that can be evaluated exactly:

$$\Xi = e^{-G_{\rm perf}/k_BT}\left(1+e^{-\Delta G_{\rm vac}/k_BT}+e^{-\Delta G_{\rm mis}/k_BT}\right)^N \quad [8]$$

With the partition function in hand, the probability of the *single* perfect capsid configuration is given by which is used below to study more general spherical capsids, beyond HBV. A plot of (9) is given in figure S5a in the Supporting Information, as are additional virial-like corrections to the isolated defect approximation.

Application to the hepatitis B virus capsid. We apply the lattice model to study the HBV $T = 4$ capsid through its contact graph. The capsid is composed of 120 dimers, each of which consists of a pair of subunits, each contributing a pair of helices to the 4-helix bundle interface and further linked by a disulfide bridge. We considered each dimer to constitute a site in our model. We constructed the contact graph $\mathcal{G}$ for the virus from the structure of the capsid given in the PDB (code 1QGT)(60) by including an edge for each pair of dimers in which there is at least one pair of α carbons within 10 Å of each other in the complete structure of the capsid. In this graph there are 4 nearest neighbors for each site.

D. Numerical computations. In addition to the analytical approximation just given, we study the full model of Sec. B using Metropolis Monte Carlo (MC) simulation. In Metropolis MC, trial moves attempt to change the configuration and are accepted with probability $\min(1, \exp[-\beta\Delta H(\mathbf{x})])$ where $H(\mathbf{x})$ is the appropriate grand-canonical potential corresponding to Eq. (3) defined by

$$H(\mathbf{x}) = G(\mathbf{x}) - \mu N(\mathbf{x}) = -\mu N(\mathbf{x}) + \sum_{\text{edges}\ ij\in\mathcal{G}} \Delta G_{\rm int}(x_i, x_j) \quad [10]$$

where N is the total number of subunits and ΔH is the change in H in going from an old to a new configuration.

We performed a set of MC simulations for our model as applied to the hepatitis B capsid, using the contact graph $\mathcal{G}$ constructed from its structure as described above. Monte Carlo simulations of the model were performed with varying values of μ, $\Delta G_{\rm ideal}$, and $\Delta G_{\rm mixed}$ to map out a "phase diagram" for the system. The MC moves for these simulations consisted of choosing a site i at random and changing its state. Each simulation lasted for 1 billion trial moves, and the average number and distribution of the number of occupied sites were computed. The simulations were performed on a grid in μ-$\Delta G_{\rm ideal}$-$\Delta G_{\rm mixed}$ space in which μ ranged from $-6k_BT$ to $6k_BT$ in steps of $0.2k_BT$, $\Delta G_{\rm ideal}$ ranged from $-5k_BT$ to 0 in steps of $0.25k_BT$, and $\Delta G_{\rm mixed}$ ranged from $\Delta G_{\rm ideal}$ to 0 in steps of $0.25k_BT$. Only simulations in which $|\Delta G_{\rm mixed}| \le |\Delta G_{\rm ideal}|$ were run.

To be considered a "partially formed capsid," a collection of subunits must be touching each other, so that they would be expected to move together because of the forces holding them together, but independently of any other collection of subunits. Consequently, for the purposes of analyzing this simulation, a "partially formed capsid" was defined as a set of occupied sites (either ideally occupied or mis-occupied) that span a connected subgraph of the contact graph $\mathcal{G}$. Therefore, after each trial move of the simulation, the subgraph of $\mathcal{G}$ spanned by the occupied sites was determined and divided into connected components. The distribution of the sizes of these subcomponents was then used for further analysis. The

DRAFT

probability of perfect capsids (in which every site is ideally occupied) was determined separately.

5. Acknowledgments

Access to the HBV cryoEM data was kindly granted by Dr. Alasdair Steven, NIH. We also thank Drs. David Koes, Lillian Chong, Barmak Mostofian, and Jeremy Copperman for helpful discussions and technical assistance. We also thank the Advanced Computing Center at OHSU for computer time. This work was supported by NIH grants 1R01-GM115805 and R21-AI130745, and by NSF grants MCB-1715823 and CNS-1229064.

1. Perlmutter JD, Hagan MF (2015) Mechanisms of virus assembly. *Annu. Rev. Phys. Chem.* 66:217–39.
2. Mateu MG (2013) Assembly, stability and dynamics of virus capsids. *Arch. Biochem. Biophys.* 531:65–79.
3. Gibson W, Roizman B (1972) Proteins specified by herpes-simplex virus .8. characterization and composition of multiple capsid forms of subtypes 1 and 2. *J. Virol.* 10(5):1044–1052.
4. Homa FL, et al. (2013) Structure of the pseudorabies virus capsid: Comparison with herpes simplex virus type 1 and differential binding of essential minor proteins. *J. Mol. Biol.* 425(18):3415–3428.
5. Caspar DLD, Klug A (1962) Physical principles in the construction of regular viruses. *Cold Spring Harbor Symp. Quant. Biol.* 27:1–24.
6. Zlotnick A, et al. (1996) Dimorphism of hepatitis B virus capsids is strongly influenced by the C-terminus of the capsid protein. *Biochemistry* 35(23):7412–7421.
7. Watts NR, et al. (2002) The morphogenic linker peptide of hbv capsid protein forms a mobile array on the interior surface. *EMBO J.* 21(5):876–884.
8. DiMattia MA, et al. (2013) Antigenic switching of hepatitis B virus by alternative dimerization of the capsid protein. *Structure* 21(1):133–142.
9. Lavelle L, et al. (2009) Phase diagram of self-assembled viral capsid protein polymorphs. *J. Phys. Chem. B* 113(12):3813–3819.
10. Chang J, Liu XA, Rochat RH, Baker ML, Chiu W (2012) *Reconstructing Virus Structures from Nanometer to Near-Atomic Resolutions with Cryo-Electron Microscopy and Tomography*, Advances in Experimental Medicine and Biology. (Springer-Verlag Berlin, Berlin) Vol. 726, pp. 49–90.
11. Veesler D, Kearney BM, Johnson JE (2016) Integration of x-ray crystallography and electron cryo-microscopy in the analysis of virus structure and function. *Crystallogr. Rev* 22(2):102–127.
12. Conway JF, et al. (1997) Visualization of a 4-helix bundle in the hepatitis B virus capsid by cryo-electron microscopy. *Nature* 386(6620):91–94.
13. Rhodes G (2006) *Crystallography made Crystal Clear, 3rd ed.* (Elsevier Academic Press).
14. Nogales E, Scheres SHW (2015) Cryo-em: A unique tool for the visualization of macromolecular complexity. *Mol. Cell* 58(4):677–689.
15. Cheng Y, Grigorieff N, Penczek PA, Walz T (2015) A primer to single-particle cryo-electron microscopy. *Cell* 161(3):438–449.
16. Conway JF, Steven AC (1999) Methods for reconstructing density maps of single particles from cryoelectron micrographs to subnanometer resolution. *Journal of Structural Biology* 128(1):106–118.
17. Wingfield PT, Stahl SJ, Williams RW, Steven AC (1995) Hepatitis core antigen produced in escherichia coli: Subunit composition, conformational analysis, and in vitro capsid assembly. *Biochemistry* 34(15):4919–4932.
18. Ceres P, Zlotnick A (2002) Weak protein-protein interactions are sufficient to drive assembly of hepatitis B virus capsids. *Biochemistry* 41(39):11525–11531.
19. Kukreja AA, et al. (2014) Structurally similar woodchuck and human hepadnavirus core proteins have distinctly different temperature dependences of assembly. *J. Virol.* 88(24):14105–14115.
20. Schwartz R, Shor PW, Peter E. Prevelige J, Berger B (1998) Local rules simulation of the kinetics of virus capsid self-assembly. *Biophys. J.* 75:2626–2636.
21. Baschek JE, Klein HCR, Schwarz US (2012) Stochastic dynamics of virus capsid formation: direct versus hierarchical self-assembly. *BMC Biophysics* 5.
22. Xie L, Smith GR, Feng X, Schwartz R (2012) Surveying capsid assembly pathways through simulation-based data fitting. *Biophys. J.* 103:1545–1554.
23. Perkett MR, Hagan MF (2014) Using markov state models to study self-assembly. *J. Chem. Phys.* 140:214101.
24. Dykeman EC, Stockley PG, Twarock R (2014) Solving a levinthals paradox for virus assembly identifies a unique antiviral strategy. *Proc. Natl. Acad. Sci. USA* 111(14):53615366.
25. Nguyen HD, Reddy VS, Brooks III CL (2007) Deciphering the kinetic mechanism of spontaneous self-assembly of icosahedral capsids. *Nano Lett.* 7(2):338–344.
26. Nguyen HD, Brooks III CL (2008) Generalized structural polymorphism in self-assembled viral particles. *Nano Lett.* 8(12):45744581.
27. Nguyen HD, Reddy VS, Brooks III CL (2009) Invariant polymorphism in virus capsid assembly. *J. Am. Chem. Soc.* 131:2606–2614.
28. Hagan MF, Chandler D (2006) Dynamic pathways for viral capsid assembly. *Biophys. J.* 91:42–54.
29. Panahandeh S, Li SY, Zandi R (2018) The equilibrium structure of self-assembled protein nano-cages. *Nanoscale* 10(48):22802–22809.
30. Spiriti J, Zuckerman DM (2015) Tabulation as a high-resolution alternative to coarse-graining protein interactions: Initial application to virus capsid subunits. *J. Chem. Phys.* 143:243159.
31. Zlotnick A (1994) To build a virus capsid - an equilibrium-model of the self-assembly of polyhedral protein complexes. *J. Mol. Biol.* 241(1):59–67.
32. Bruinsma RF, Gelbart WM, Reguera D, Rudnick J, Zandi R (2003) Viral self-assembly as a thermodynamic process. *Phys. Rev. Lett.* 90(24):4.
33. Zandi R, van der Schoot P, Reguera D, Kegel W, Reiss H (2006) Classical nucleation theory of virus capsids. *Biophys. J.* 90(6):1939–1948.
34. Bruinsma RF, Klug WS (2015) Physics of viral shells. *Annual Review of Condensed Matter Physics, Vol 6* 6:245–268.
35. Chen JZ, Chevreuil M, Combet S, Lansac Y, Tresset G (2017) Investigating the thermal dissociation of viral capsid by lattice model. *J. Phys.-Condes. Matter* 29(47):8.
36. Tresset G, et al. (2017) Two-dimensional phase transition of viral capsid gives insights into subunit interactions. *Phys. Rev. Appl.* 7(1):8.
37. Zlotnick A, Johnson JM, Wingfield PW, Stahl SJ, Endres D (1999) A theoretical model successfully identifies features of hepatitis B virus capsid assembly. *Biochemistry* 38(44):14644–14652.
38. Chandler D (1987) *Introduction to Modern Statistical Mechanics.* (Oxford University Press, USA).
39. Pathria RK (1996) *Statistical Mechanics.* (Elsevier, Amsterdam).
40. Metropolis N, Rosenbluth AW, Rosenbluth MN, Teller AH, Teller E (1953) Equation of state calculations by fast computing machines. *J. Chem. Phys.* 21(6):1087–1092.
41. Heymann JB, et al. (2003) Dynamics of herpes simplex virus capsid maturation visualized by time-lapse cryo-electron microscopy. *Nat. Struct. Mol. Biol.* 10(5):334–341.
42. Gao HX, Valle M, Ehrenberg M, Frank J (2004) Dynamics of ef-g interaction with the ribosome explored by classification of a heterogeneous cryo-em dataset. *Journal of Structural Biology* 147(3):283–290.
43. Leschziner AE, Nogales E (2007) *Visualizing flexibility at molecular resolution: Analysis of heterogeneity in single-particle electron microscopy reconstructions*, Annual Review of Biophysics. (Annual Reviews, Palo Alto) Vol. 36, pp. 43–62.
44. Bilokapic S, Strauss M, Halic M (2018) Cryo-em of nucleosome core particle interactions in trans. *Sci Rep* 8:8.
45. Eisenstein M (2006) Adventures in the matrix. *Nat. Methods* 3:410.
46. Zimm BH (1948) Apparatus and methods for measurement and interpretation of the angular variation of light scattering; preliminary results on polystyrene solutions. *The Journal of Chemical Physics* 16(12):1099–1116.
47. Tang C, et al. (2003) Antiviral inhibition of the hiv-1 capsid protein. *J. Mol. Biol.* 327(5):1013–1020.
48. Neira JL (2009) The capsid protein of human immunodeficiency virus: designing inhibitors of capsid assembly. *FEBS J.* 276(21):6110–6117.
49. Pak AJ, Grime JMA, Yu A, Voth GA (2019) Off-pathway assembly: A broad-spectrum mechanism of action for drugs that undermine controlled hiv-1 viral capsid formation. *J. Am. Chem. Soc.* 141(26):10214–10224.
50. Deres K, et al. (2003) Inhibition of hepatitis B virus replication by drug-induced depletion of nucleocapsids. *Science* 299(5608):893–896.
51. Stray SJ, Johnson JM, Kopek BG, Zlotnick A (2006) An in vitro fluorescence screen to identify antivirals that disrupt hepatitis B virus capsid assembly. *Nat. Biotechnol.* 24(3):358–362.
52. Cho MH, Jeong H, Kim YS, Kim JW, Jung G (2014) 2-amino-N-(2,6-dichloropyridin-3-yl)acetamide derivatives as a novel class of HBV capsid assembly inhibitor. *J. Viral Hepatitis* 21(12):843–852.
53. Shi J, Zhou J, Shah VB, Aiken C, Whitby K (2011) Small-molecule inhibition of human immunodeficiency virus type 1 infection by virus capsid destabilization. *J. Virol.* 85(1):542–549.
54. Stray SJ, Zlotnick A (2006) BAY 41-4109 has multiple effects on hepatitis B virus capsid assembly. *J. Mol. Recognit.* 19(6):542–548.
55. Qazi S, Schlicksup CJ, Rittichier J, VanNieuwenhze MS, Zlotnick A (2018) An assembly-activating site in the hepatitis B virus capsid protein can also trigger disassembly. *ACS Chem. Biol.* 13(8):2114–2120.
56. Scheres SHW (2012) Relion: Implementation of a bayesian approach to cryo-em structure determination. *Journal of Structural Biology* 180(3):519–530.
57. Scheres SHW (2012) A bayesian view on cryo-em structure determination. *J. Mol. Biol.* 415(2):406–418.
58. Zuckerman DM (2010) *Statistical Physics of Biomolecules: An Introduction.* (CRC Press, Boca Raton, FL).
59. Hill TL (1986) *An introduction to statistical thermodynamics.* (Dover Publications, Inc., New York).
60. Wynne SA, Crowther RA, Leslie AGW (1999) The crystal structure of the human hepatitis B virus capsid. *Mol. Cell* 3(6):771–780.

DRAFT

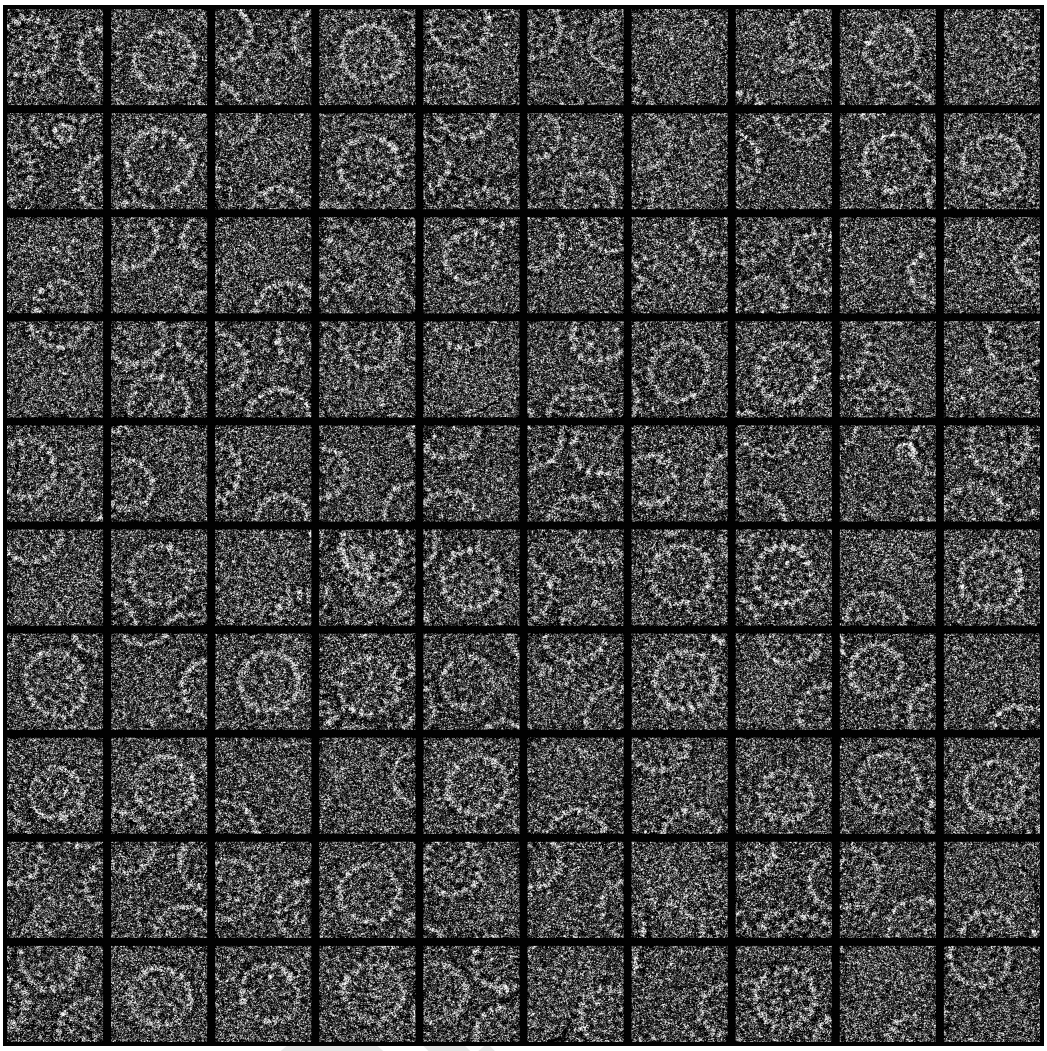

Fig. S1. Sample of 100 images of the HBV capsid taken from the entire stack.

6. Supporting Information

A. Samples and descriptions of cryo-EM images of HBV capsids.

Description	Images
Partial capsids	1, 3, 5, 6, 8, 10, 11, 13, 15-18, 21-23, 26-36, 39, 40-50, 51, 53, 56, 59, 62, 66, 68, 70, 73, 74, 76, 77, 81-83, 85, 86, 88-91, 95-97, 99, 100
No visible capsid	7, 24, 87
Missing dimer	19, 20, 37, 38, 58, 60, 66, 72
Small	25, 69, 71, 78
Small with missing dimer	9, 65, 67, 84, 93
Elongated	57, 61

Table S1. Description of defects in the sample of 100 images drawn from the entire stack. The images are numbered such that images 1-10 correspond to the top row of figure S1, 11-20 to the second row, and so on.

DRAFT

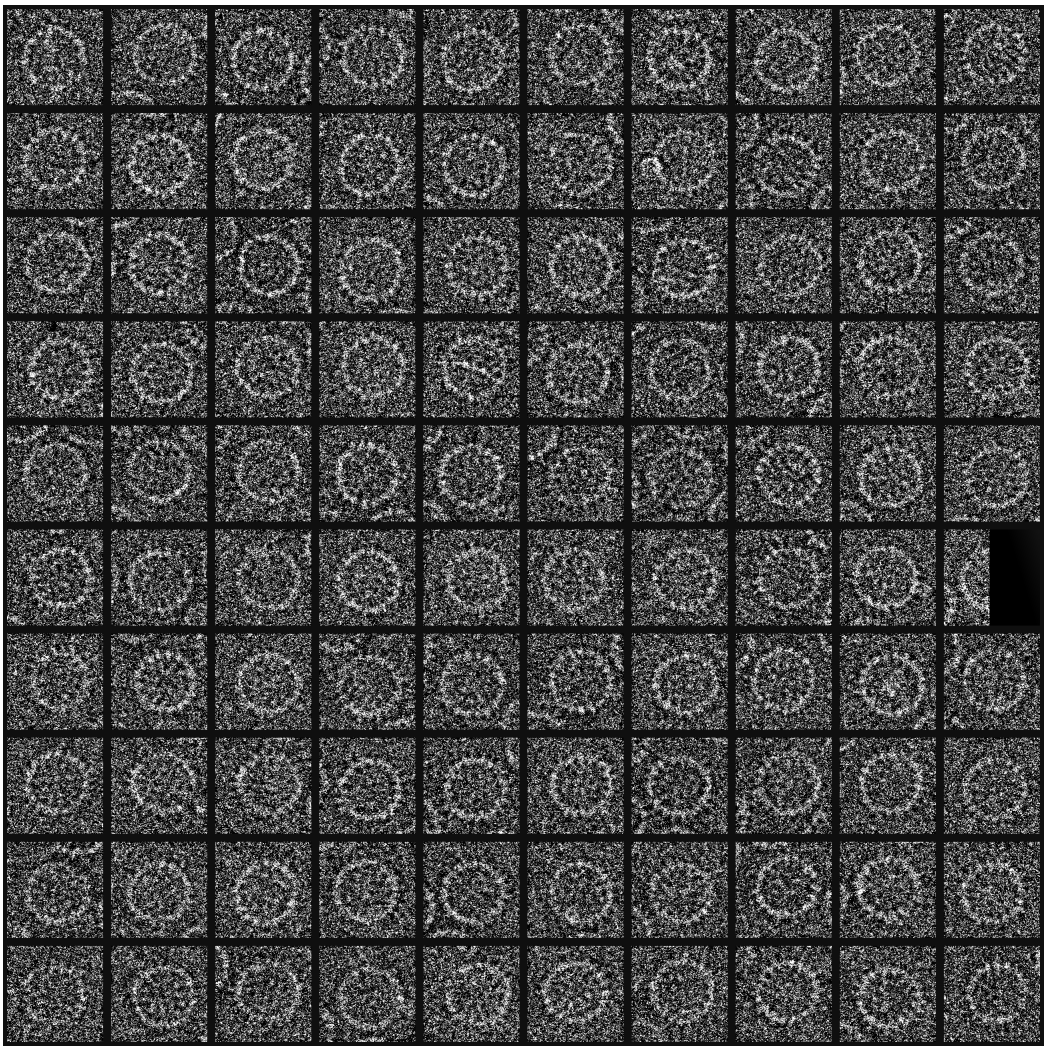

Fig. S2. Sample of 100 images of the HBV capsid taken from the filtered stack.

Description	Images
Missing dimer	1, 18, 22, 58, 72, 89, 95
Missing multiple dimers	16, 42
Extra lines across capsid	35
Additionally attached dimer, "bud", or other extra appendage	7, 13, 17, 27, 53, 69, 86
Partially obscured by gray rectangle	60

Table S2. Description of defects in the sample of 100 images drawn from the filtered stack of 4940 images created by 2D classification. The images are numbered such that images 1-10 correspond to the top row of figure S2, 11-20 to the second row, and so on.

DRAFT

$$
\begin{aligned}
\frac{\Xi}{\exp[-G_{\mathrm{perf}}/k_BT]} &= (1+z_v+z_m)^{120} - 240z_v^2(1+z_v+z_m)^{113} + \\
&\quad 240\exp[-(2\mu-7\Delta G_{\mathrm{ideal}})](1+z_v+z_m)^{113} \\
&= (1+z_v+z_m)^{120} - \\
&\quad 240z_v^2[\exp(-\Delta G_{\mathrm{ideal}})-1](1+z_v+z_m)^{113}
\end{aligned}
$$

Virial-like corrections to the isolated-defect approximation for the lattice model

Given a specific contact graph $\mathcal{G}$, the approximate analytical approach to the lattice model described in the main text of the paper may be extended to incorporate defects that are not isolated. This is done by incorporating additional terms in higher powers of the fugacities z_v and z_m of defects involving vacant or mis-occupied sites, which are defined as $z_v = \exp[-\Delta G_{\mathrm{vac}}/k_BT]$ and $z_m = \exp[-\Delta G_{\mathrm{mis}}/k_BT]$. For example, in the hepatitis B capsid, of the $120!/(2!\,118!) = 7140$ configurations with exactly two empty sites, 240 have the sites touching each other. The difference in energy between these configurations and the perfect capsid is $2\mu - 7\Delta G_{\mathrm{ideal}}$, not $2\mu - 8\Delta G_{\mathrm{ideal}}$, which would be the energy difference associated with two isolated empty sites. This is because a defect of this type removes the interactions among only seven edges rather than eight (see figure S3). Thus the correction to Ξ needed to account for defects of this type is given by where the second term in the first line subtracts out the incorrect terms in Ξ and the third term replaces them with the correct terms. The factor of $(1+z_v+z_m)^{113}$ accounts for the possibility of isolated defects among the 113 sites not occupied by or touching the two empty sites that are together. In addition to this, two other correction terms in z_vz_m and z_m^2 would be needed to account for defects in which one of the touching sites was partially attached and the other empty, or both partially attached. Additional terms in higher powers of z_v or z_m would be needed for defects involving three or more sites touching each other.

This approach is very reminiscent of the well-known virial expansion,(38, 39), where the effect of intermolecular forces in a real gas can be expressed as correction terms in powers of the density, relative to the partition function of an ideal gas. These correction terms can be determined using cluster diagrams. For viruses, the correction terms depend on the details of the contact graph and the particular defects that are possible, and can be derived in a similar manner to the example given above.

Additional results from Monte Carlo simulations of the lattice model

DRAFT

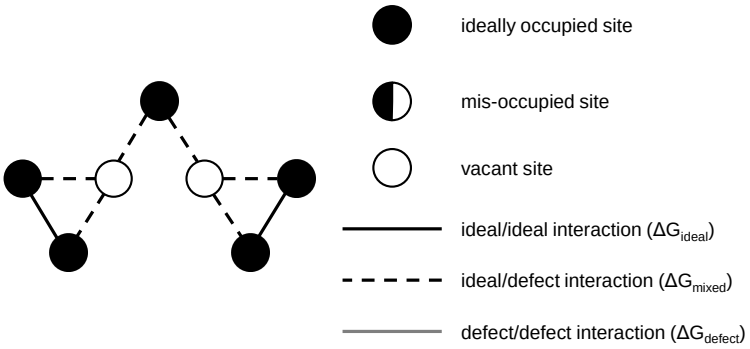

Fig. S3. Example of a defect in the HBV capsid that consists of two neighboring vacant sites surrounded by occupied sites and therefore violates the isolated-defects approximation used in the analytical treatment of the lattice model described in the main text. The analytical treatment may be extended to cover this case by using a virial-like expansion.

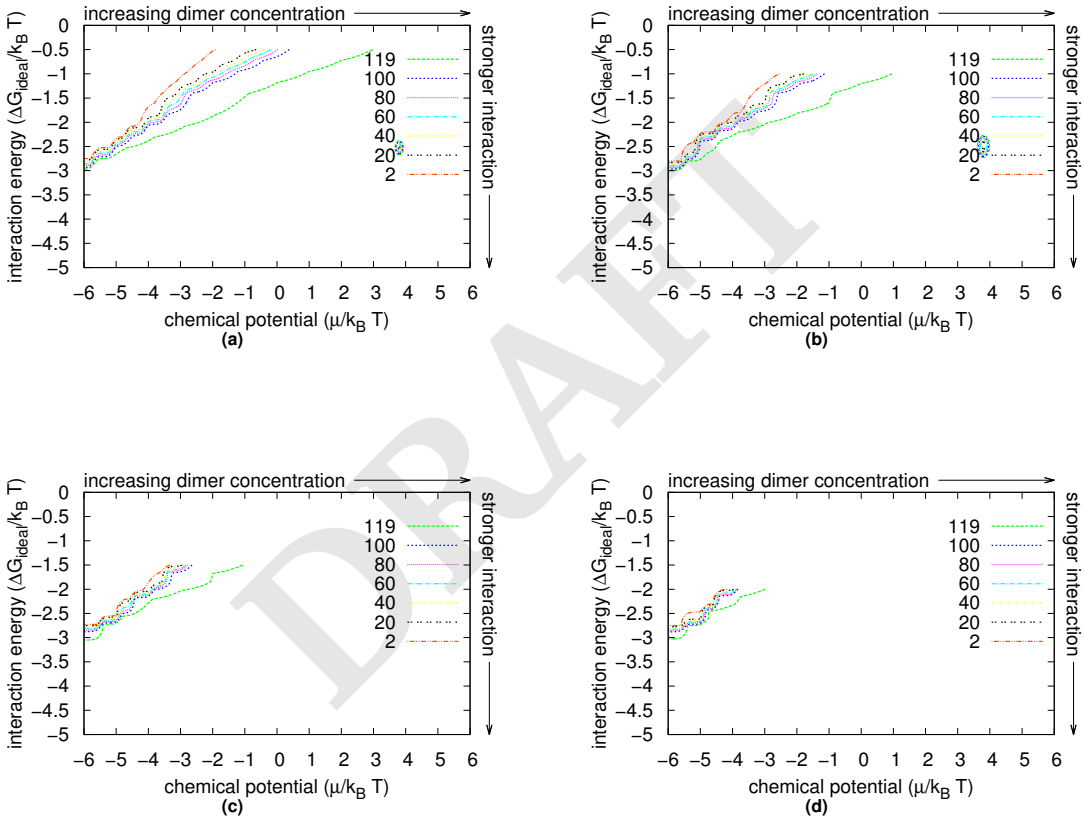

Fig. S4. Dependence of capsid formation on chemical potential μ and interaction strength $\Delta G_{\mathrm{ideal}}$. Contour plot of the average connected capsid size (including mis-occupied sites) in Monte Carlo simulations of our model on the hepatitis B virus contact graph in the $(\mu, \Delta G_{\mathrm{ideal}})$ plane as in figure 4 for (a) $\Delta\Delta G = 0.5 k_B T$; (b) $\Delta\Delta G = 1.0 k_B T$; (c) $\Delta\Delta G = 1.5 k_B T$; (d) $\Delta\Delta G = 2.0 k_B T$.

DRAFT

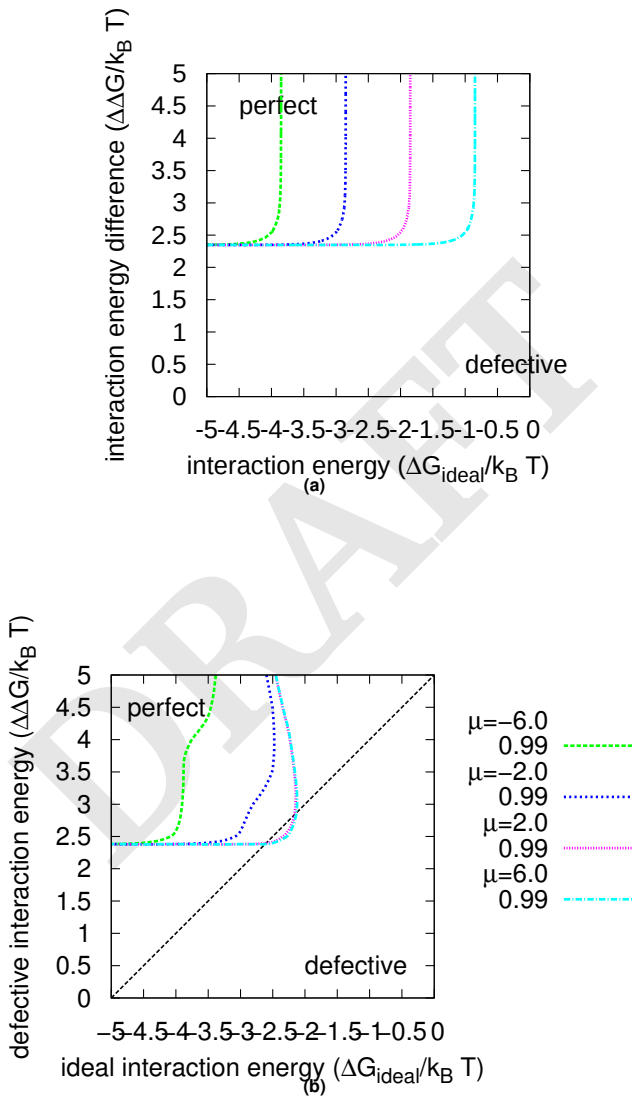

Fig. S5. When are perfect capsids expected? (a) Plot of $p_{\text{perfect capsid}}$ as determined from equation 9 and (b) $p_{\text{perfectcapsid}}$, as determined from MC simulations, both showing the position of the 0.99 contour in the $(\Delta G_{\text{ideal}}, \Delta\Delta G)$ space (chemical potential and interaction energy). Different curves show this contour for different values of the chemical potential μ.

DRAFT

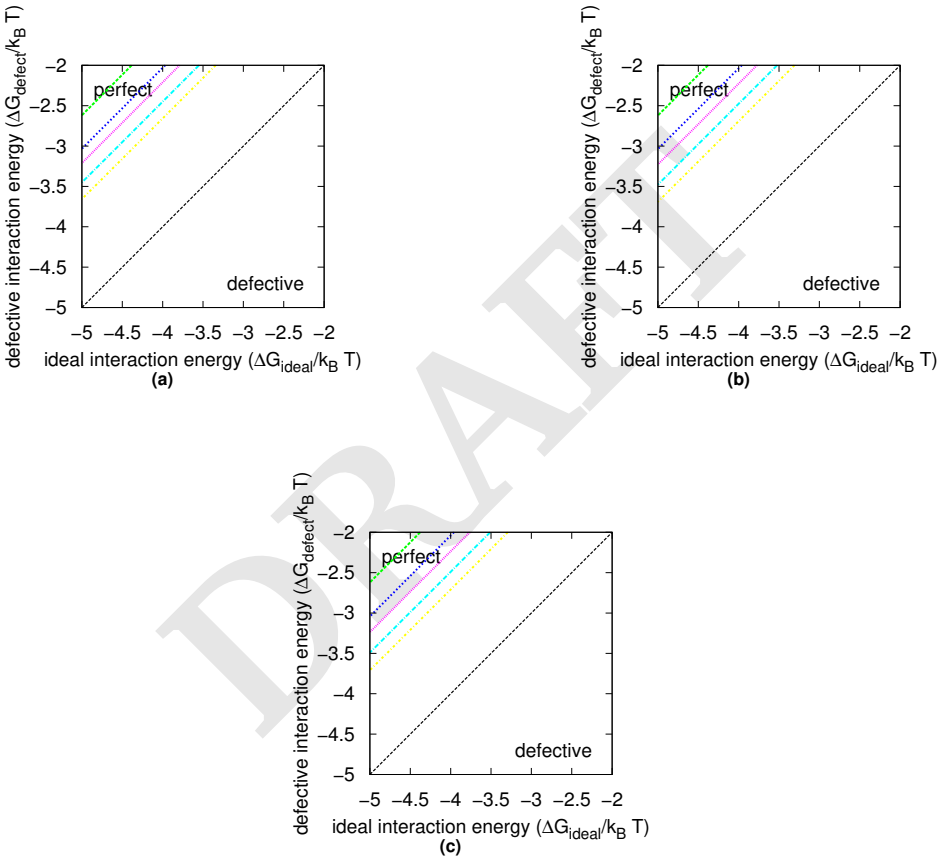

Fig. S6. Effect of $\Delta G_{\mathrm{defect}}$ on the probability of perfect capsids. Probability of perfect capsids in the $(\Delta G_{\mathrm{ideal}}, \Delta G_{\mathrm{mixed}})$ plane as determined from MC simulations with different values of $\Delta G_{\mathrm{defect}}$. (a) for $\Delta G_{\mathrm{defect}} = \Delta G_{\mathrm{ideal}} + 0.1 k_B T$; (b) for $\Delta G_{\mathrm{defect}} = \Delta G_{\mathrm{ideal}} + 1.0 k_B T$; (c) for $\Delta G_{\mathrm{defect}} = \Delta G_{\mathrm{ideal}} + 10.0 k_B T$.

DRAFT